

## Research Paper

## Assessment of COVID-19 aerosol transmission in a university campus food environment using a numerical method

M. Zhao<sup>a</sup>, C. Zhou<sup>a</sup>, T. Chan<sup>b</sup>, C. Tu<sup>a</sup>, Y. Liu<sup>c</sup>, M. Yu<sup>a,\*</sup><sup>a</sup> Laboratory of Aerosol Science and Technology, China Jiliang University, Hangzhou, China<sup>b</sup> Department of Mechanical Engineering, The Hong Kong Polytechnic University, Kowloon, Hong Kong, China<sup>c</sup> College of Modern Science, China Jiliang University, Hangzhou, China

## ARTICLE INFO

## Article history:

Received 13 August 2021

Revised 30 November 2021

Accepted 20 January 2022

Available online 21 January 2022

## Keywords:

COVID-19 transmission

University dining hall

Cough

Table partition

Computational fluid dynamics

## ABSTRACT

With the prevalence of COVID-19, the phenomenon of viruses spreading through aerosols has become a focus of attention. Diners in university dining halls have a high risk of exposure to respiratory droplets from others without the protection of face masks, which greatly increases the risk of COVID-19 transmission. Therefore, the transmission mechanism of respiratory droplets in extremely crowded dining environments should be investigated. In this study, a numerical simulation of coughing at dining tables under two conditions was performed, namely the presence and absence of protective partitions, and the evaporation and condensation of aerosol droplets in the air were examined. By using the numerical method, we analyzed and verified the isolation effect of dining table partitions in the propagation of aerosol droplets. The effect of changes in room temperature on the diffusion of coughed aerosols when partitions were present was analyzed. We demonstrated how respiratory droplets spread through coughing and how these droplets affect others. Finally, we proposed a design for a dining table partition that minimizes the transmission of COVID-19.

© 2021 China University of Geosciences (Beijing) and Peking University. Production and hosting by Elsevier B.V. This is an open access article under the CC BY-NC-ND license (<http://creativecommons.org/licenses/by-nc-nd/4.0/>).

## Abbreviations

## a. Nomenclature

$F_D$	Drag force per unit mass of the particle
$U$	Fluid speed
$u_p$	Speed of the particles
$d_p$	Diameter of the particle
$Re$	Relative Reynolds number
$C_D$	Drag coefficient of the particle
$m_p$	Mass of the particle
$v_i$	Velocity of the particle
$F_s$	Saffman lift of a single particle
$H$	Convective heat transfer coefficient
$T_{f1}$	Temperature of the ambient air, K
$T_{f2}$	Temperature of the droplets, K
$Nu$	Nusselt number
$k$	Thermal conductivity of air

$Pr$	Prandtl number of air
$C_p$	Specific heat capacity of a droplet
$h_{fg}$	Enthalpy of phase change in joules per kilogram
$u_\infty$	Speed of humid air
$N_i$	The molar flux of convective mass transfer
$M_{w,i}$	The molar mass of the $i$ th component
$k_c$	Mass transfer coefficient
$C_{i,s}$	Water vapor concentration on the surface of a droplet
$C_{i,\infty}$	Water vapor concentration in ambient air
$P_{sat}$	Saturated vapor pressure of a water droplet at temperature $T_p$
$R$	Universal gas constant
$X_i$	Mole fraction of water in the air
$P$	Absolute pressure of the air
$Sh_{AB}$	Sherwood number
$D_{i,m}$	Diffusion coefficient of water in humid air
$Sc$	Schmidt number

\* Corresponding author.

E-mail address: [mzyu@cju.edu.cn](mailto:mzyu@cju.edu.cn) (M. Yu).

(continued on next page)

$B_m$	Spalling mass
$Y_{i,s}$	Mass fraction of water vapor on the surface of the droplet
$Y_{i,\infty}$	Mass fraction of water in the air
$N_p$	Number of particles
$R_p$	Particle arrival ratio
b. Greek letters	
$\mu$	Dynamic viscosity of the fluid
$\rho$	Fluid density
$\rho_p$	Particle density
$g$	Acceleration of gravity, m/s <sup>2</sup>
$\Phi$	Total heat transferred, J
$A_p$	The surface area of the aerosol droplets, m <sup>2</sup>
c. Abbreviations	
COVID-19	Coronavirus pneumonia termed coronavirus disease 2019
CFD	Computational fluid dynamics
DPM	Discrete particle model
SARS-CoV-2	Acute respiratory condition coronavirus 2

## 1. Introduction

Since December 31, 2019, a new type of coronavirus, i.e. coronavirus disease 2019 (COVID-19), has had a substantial effect on humans and has threatened global health, but our understanding of the transmission of the virus on various occasions is not comprehensive. Therefore, the spread of the new coronavirus and the laws related to the spread, which are crucial to the prevention and control of the epidemic worldwide, require urgent investigation.

The WHO has confirmed that the virus can spread from an infected person's mouth or nose in small liquid particles when they cough, sneeze, speak, sing or breathe. These particles range from larger respiratory droplets to smaller aerosols ("Coronavirus disease (COVID-19)", n.d.). Although experimental research can yield reliable results (Schade et al., 2021a, b), the cost of an experiment in this context would be high, and information regarding droplet migration during the propagation of aerosol droplets is not easy to be collected. In addition, obtaining the interaction of droplet transmission and field information, including pressure field and temperature field of a given space, would be challenging. Today, awareness of the aerosol transmission of the virus has increased. The aerosol transmission from a fluid flow viewpoint has been studied and reviewed since the appearance of SARS-CoV-2 (Mingotti et al., 2020; Bourouiba, 2021; Schade et al., 2021a, b).

With the development of numerical calculation methods and the rapid improvement in the performance of computer calculations, computational fluid dynamics (CFD) has become the backbone of scientific research and engineering applications. Zhao et al. (2004) used CFD to simulate the diffusion of aerosol droplets in a room under different ventilation conditions. The results indicated that the human body expels numerous droplets when coughing and that they can spread and remain suspended in the air. The study also indicated that proper ventilation conditions can quickly eliminate these droplets (Zhao et al., 2004). Li et al. (2003) performed a numerical simulation to study the movement of aerosol droplets during periodic coughing. The study revealed that aerosol droplets are mainly driven by cough-related airflow. After a cough, drag force and inertia cause droplets to continue moving forward. By comparing the propagation distance of aerosol droplets during a single cough with that of periodic coughing, that study discovered that periodic coughing can carry aerosol droplets farther than can a single cough (Li et al., 2003).

The effect of evaporation on aerosol transmission has drawn the attention of community of computational fluid dynamics. Ji et al. (2018) performed a numerical simulation to calculate the evaporation rate of aerosol droplets in different ventilated environments. The results indicated that smaller droplets are less affected by ventilation than larger ones are. The lower the wind speed, the slower the evaporation rate of the droplets but the faster the sedimentation rate (Ji et al., 2018). Liu et al. (2017) performed a numerical simulation of the evaporation of droplets of different sizes at different temperatures and humidity. The study revealed that the presence of turbulence increased the residence time of droplets in the air, especially for particles with large diameters. The droplets were highly sensitive to the relative humidity of the environment, but smaller droplets were less sensitive to relative humidity and quickly formed droplet nuclei after evaporation (Liu et al., 2017). Busco et al. (2020) used numerical simulation methods to conduct numerous computational studies on human sneezing. The research revealed that either the deposition rate or the evaporation rate of the droplets in the traditional model were faster than the actual rates were. The droplets in the traditional model exhibited less evaporation and more deposition than actual droplets did. In addition, the study revealed that cold, dry environments caused a larger mass percentage of droplet evaporation (Busco et al., 2020). Feng et al. (2020) used CFD to study the spread of SARS-CoV-2 through the air. The study revealed that the transport of droplets by wind is complicated and highly dependent on the local flow field and wake flow pattern. The study also confirmed that 1.8 m is an insufficient distance to protect people from the spread of viruses through coughing (Feng et al., 2020).

According to a World Health Organization report, SARS-CoV-2 is mainly spread through close contact, aerosols, and various other forms of transmission (Galbadage et al., 2020). Aerosol droplets carrying the virus may originate from the respiratory behaviors of infected individuals when speaking, sneezing, or coughing (Busco et al., 2020). In crowded public areas, such as schools, stations, and restaurants, the risk of aerosol transmission of the virus sharply increases. Restaurants are among the most visited areas of schools. Therefore, the prevention and control of the pandemic in university dining halls are essential. Since the appearance of SARS-CoV-2, the use of partitions on dining tables is a common way to prevent and control SARS-CoV-2 in almost all countries' school dining rooms. In this article, we use a novel numerical method for multiphase flows to assess whether this way is reliable. To achieve this, the discrete particle model (DPM) and the component transport model were used to explore the effects of partitions on the diffusion of aerosol droplets through coughing and determine whether such partitions can effectively prevent droplets from spreading between two diners. In the implementation of the DPM, the Evaporation model which accounts for both heat and mass transfer between the surrounding air and droplets is utilized. Changes in seasons and weather were considered to explore the effect of ambient temperature, which influences the number of droplets suspended in the air and their proliferation, on the evaporation of aerosols with the partition installed.

## 2. Mathematical model

The aerosol transmission due to cough is a complicated multiphase flow process, which involves flow convection and diffusion, and also the evolution of aerosol droplets dynamics, including droplets evaporation and condensation (Bourouiba, 2021). In the study of multiphase flow, the two-phase flow method is the approach most commonly used to study aerosol droplet diffusion. The two-phase flow method consists of two methods of description. The first involves treating the fluid as a continuous medium and the

particles as a pseudo-fluid, and the second involves treating the fluid as a continuous medium and the particles as discrete units. The numerical simulation consists of two methods. The first is the Euler–Euler method, which treats the liquid particles in a flow field as a pseudo-fluid and uses the Euler coordinate system to express the liquid particles and the air phase fluid. The second is the well-known Euler–Lagrangian method, which uses the Euler method to describe the air continuous phase fluid, and the liquid particles are described by Lagrangian coordinates.

In this study, the well-known Euler–Lagrangian method, i.e. discrete particle model (DPM), is used (Sokolichin et al., 1997). The classical turbulence model,  $k$ – $\varepsilon$  turbulence model, is utilized to resolve the Navier–Stokes equation, which describes the continuous air phase. All the calculation is implemented in the platform of Ansys software, i.e. FLUENT.

### 2.1. Discrete particle model

When the trajectory of a particle's motion is determined by using the differential equation for particle action, the force balance equation for a particle in the Cartesian  $x$ -coordinate system is as follows:

$$\frac{du_p}{dt} = F_D(u - u_p) + \frac{g_x(\rho_p - \rho)}{\rho_p} + F_x \quad (1)$$

where  $u$  is the fluid speed,  $u_p$  is the speed of the particles,  $\rho$  is the fluid density,  $\rho_p$  is the particle density,  $g_x$  is the acceleration of gravity,  $F_x$  is the sum of body forces. In Eq. (1), the first term on the right side of the equation is the drag force per unit mass of the particle, where

$$F_D = \frac{18\mu C_D Re}{\rho_p d_p^2} \frac{C_D Re}{24} \quad (2)$$

where  $\mu$  is the dynamic viscosity of the fluid,  $d_p$  is the diameter of the particle, and  $Re$  is the relative Reynolds number, defined as

$$Re = \frac{\rho d_p |u_p - u|}{\mu} \quad (3)$$

In Eq. (2), the drag coefficient  $C_D$  is expressed as follows:

$$C_D = a_1 + \frac{a_2}{Re} + \frac{a_3}{Re^2} \quad (4)$$

Where  $a_1$ ,  $a_2$ , and  $a_3$  are coefficients related to  $Re$ .

This study investigated the migration of aerosol droplets without considering the interaction force between particles and under the assumption that the density of the particles is greater than that of air. Therefore, only the gravity, drag force, and Saffman lift force,  $F_s$ , on the particles were considered; the dynamic equation for droplet particles is as follows:

$$m_p \frac{dv_i}{dt} = \pi \frac{d_p^2}{8} C_D \rho |u_i - v_i| (\bar{u}_i - v_i) + m_p g_i + F_s \quad (5)$$

In Eq. (5),  $m_p$  is the mass of the particle,  $v_i$  is the velocity of the particle. The three items on the right are the Stokes resistance, gravity, and Saffman lift of a single particle in sequence.

For the interaction between the discrete particle phase and the fluid, coupled calculations were used to obtain information such as the mass, momentum, and energy of the discrete phase to the flow field, which can indicate the true state of the flow field. Therefore, when the diffusion of droplets during coughing is simulated, the transport and diffusion of the droplets follow the gas–liquid two-phase flow model. With air used as the background fluid, the coupled flow in gas–liquid two-phase flow was calculated using the

motion equation for air and droplet particles. This two-way coupling can yield more reliable results.

### 2.2. Evaporation model

Meholic et al. (2013) obtained the basic diffusion equation for liquid evaporation by assuming that droplets evaporated in still air (Meholic et al., 2013). They discovered through later experiments that the evaporation of a droplet is proportional to its diameter, vapor pressure, and surface tension. Spalding (1953) assumed that both the gas phase and the liquid phase were quasi-steady, that the droplet shape was an ideal sphere, and that the temperature inside droplets was uniformly distributed. A classic droplet evaporation model was proposed by ignoring the heat conducted by radiation (Spalding, 1953).

#### 2.2.1. Heat transfer process

Heat is transferred between aerosol droplets and air in two stages. The first stage is the convective heat transfer between aerosol droplets and air, and the second stage is the heat exchange that occurs when droplets and air undergo mass transfer (Galdi, 2011). The left side of Eq. (6) is used to control the change in the temperature of the fluid in a control body over time. The first term on the right side of Eq. (6) is the convective heat transfer between droplets and air, and the second term is the heat exchange during mass transfer between the two.

$$m_p c_p \frac{dT_p}{dt} = h A_p (T_{f1} - T_{f2}) - \frac{dm_p}{dt} h_{fg} \quad (6)$$

where  $h$  is the convective heat transfer coefficient,  $A_p$  is the surface area of the aerosol droplets,  $T_{f1}$  is the temperature of the ambient air, and  $T_{f2}$  is the temperature of the droplets. The convective heat transfer between aerosol droplets and the air follows Newton's law of cooling. Heat transfer is expressed by the following equation:

$$\phi = h A_p (T_{f1} - T_{f2}) \quad (7)$$

The convective heat transfer coefficient is the key to the calculation. Usually, the convective heat transfer coefficient is calculated using the Nusselt number between droplets and the air (Jamil et al., 2012). Generally, the mathematical expression for spherical particles is as follows:

$$Nu = \frac{h d_p}{k} = 2 + 0.6 \times Re^{\frac{1}{2}} \times Pr^{\frac{1}{3}} \quad (8)$$

In Eq. (8),  $d_p$  is the diameter of the aerosol droplet, and  $k$  is the thermal conductivity of air.  $Re$  is the Reynolds number, and  $Pr$  is the Prandtl number of air.

In the evaporation process, heat exchanged during mass transfer is calculated using the mass change rate and the phase change enthalpy of droplets.

$$m_p c_p \frac{dT_p}{dt} = - \frac{dm_p}{dt} h_{fg} \quad (9)$$

In Eq. (9),  $C_p$  is the specific heat capacity of a droplet, and  $h_{fg}$  is the enthalpy of phase change in joules per kilogram.

#### 2.2.2. Mass transfer process

The process of mass transfer between aerosol droplets and air generally consists of three stages, namely evaporation, condensation, and boiling. The evaporation and condensation stages are controlled by the law of diffusion. During boiling, the absorbed heat is used for phase change (Bernardi et al., 2009).

When the temperature of a droplet is lower than the boiling point or when the vapor pressure on the surface of a droplet is lower than the ambient pressure, the droplet will only evaporate and condense; it will not boil. The direction in which droplets

evaporate or condense (i.e., the direction of the water phase change) is controlled by the concentration of water molecules on the surface of the droplet and in the air. When the concentration of water molecules in moist air is lower than that on the surface of the droplet, Evaporation occurs and condensation occurs otherwise (Nakano and Hashimoto, 2020).

When the mass transfer rate of evaporation and condensation is low, this rate is controlled by the law of diffusion (Zhuchkov and Utkina, 2016). The mass transfer rate of the evaporation of droplets and the condensation of water in humid air is given by

$$\frac{dm_p}{dt} = N_i A_p M_{w,i} \quad (10)$$

where  $N_i$  is the molar flux of convective mass transfer and  $M_{w,i}$  is the molar mass of the  $i$ th component. The mass transfer rate is determined by molar flux  $N_i$  of convective mass transfer in Eq. (10), and the molar flux of convective mass transfer is given by

$$N_i = k_c (C_{i,s} - C_{i,\infty}) \quad (11)$$

where  $k_c$  is the mass transfer coefficient,  $C_{i,s}$  is the water vapor concentration on the surface of a droplet, and  $C_{i,\infty}$  is the water vapor concentration in ambient air.

The water vapor concentration on the surface of a droplet is the water vapor saturation concentration of the droplet at a certain temperature. The saturated water vapor concentration on the surface of the droplet is calculated using the ideal gas equation of state.

$$C_{i,s} = \frac{P_{\text{sat}}(T_p)}{RT_p} \quad (12)$$

In Eq. (12),  $P_{\text{sat}}$  is the saturated vapor pressure of a water droplet at temperature  $T_p$ , and  $R$  is the universal gas constant.

The mass concentration of the water in the air in which a droplet is located is also obtained using the ideal gas equation of state.

$$C_{i,\infty} = X_i \frac{p}{RT_\infty} \quad (13)$$

In Eq. (14),  $X_i$  is the mole fraction of water in the air in which a droplet is located, and  $p$  is the absolute pressure of the air.

Mass transfer coefficient  $k_c$  is related to the Sherwood number, as shown in the following formula:

$$Sh_{AB} = \frac{k_c d_p}{D_{i,m}} = 2 + 0.6 Re^{1/2} Sc^{1/3} \quad (14)$$

In Eq. (14),  $Sh_{AB}$  is the Sherwood number,  $D_{i,m}$  is the diffusion coefficient of water in humid air, and  $Sc$  is the Schmidt number.

When the mass transfer rate is high, the mass transfer process is controlled by convection and diffusion. This process is shown in the following equation:

$$\frac{dm_p}{dt} = k_c A_p \rho \ln(1 + B_m) \quad (15)$$

In Eq. (15),  $B_m$  is the spalling mass, and the spalling mass is calculated using the following formula:

$$B_m = \frac{Y_{i,s} - Y_{i,\infty}}{1 - Y_{i,s}} \quad (16)$$

where  $Y_{i,s}$  is the mass fraction of water vapor on the surface of the droplet, and  $Y_{i,\infty}$  is the mass fraction of water in the air.

### 3. Geometric model and evaporation verification

#### 3.1. Model simplification

In this work, we focus on the transport of droplets from the mouth in the air, in which the evolution of particle size distribution due to heat and mass transfer is considered. Thus, we followed the existing studies for respiratory droplets and did not consider the composition of droplets, especially the COVID 19 virus, for simplifying the numerical simulation. The spread of aerosol droplets through coughing is a highly complex multiphase process affected by uncontrollable factors, such as individual factors, the intensity and duration of a cough, and environmental parameters (Heine and Bart, 2017). To accurately simulate coughing, the spreading of droplets in the dining hall was simplified as follows:

Only the flow field after the cough was considered; inhalation before the cough was not considered. This study mainly examined the spraying of droplets during coughing and the subsequent spreading through an environment.

Only water in the droplets was considered; all other components of droplets, such as viruses and particles, were ignored. This study proceeded under the assumption that the composition of aerosol droplets generated from coughing was pure water, that the droplets evaporated or settled after leaving the mouth, and that the droplets were spherical.

The human mouth exhibits various shapes when coughing. For this study, the shape of the mouth when coughing was assumed to be round, with a hydraulic diameter of 0.02 m.

The interaction force between droplets during diffusion was ignored, and only the effects of gravity, buoyancy and drag force on the droplets were considered.

The Size distributions of expiratory droplets expelled during coughing come from the measured data in Chao et al. (2009).

#### 3.2. Establishment of a geometric model and meshing

In this study, the dining hall in universities, as shown in Fig. 1a, is selected for the research objective since this is one of the most crowded places. The objective is to study how one person's cough affects another person in a short distance, thus only the small area dominated by the exhaled air from the exhaling person rather than the entire dining hall area is considered. The flow velocity from one dinner's mouth is specified as 11.7 m/s in this study, which is far greater than the ventilation velocity of university dining halls in this small area. Thus, the background ventilation is not considered in the calculation.

The length of the table is 1,200 mm, the width is 600 mm, and the height is 900 mm. The width of the partition on the table is 700 mm, and its height is 650 mm. The human body was modeled to have a height of 1,700 mm and a sitting height of 1,250 mm. The distance between two diners is 1,350 mm. The tables and diners were modeled in two situations, with the partition, and without the partition, and the Cartesian coordinate system for modeled dining tables and diners is presented in Fig. 1b.

In the calculation, unstructured grids were used because the geometric structure was relatively complex (Corrigan et al., 2011). The number of unstructured grids was relatively high to adapt to the complex geometric structures. Fig. 2 presents the Overall meshing.

The diameter of the mouth in the sample calculation was only 0.02 m, which is small compared with the entire computational domain. The initial velocity near the mouth was as high as 11.7 m/s. Because the velocity gradient in this area was large, the mesh at the mouth and the partition were refined (Fig. 3). In other

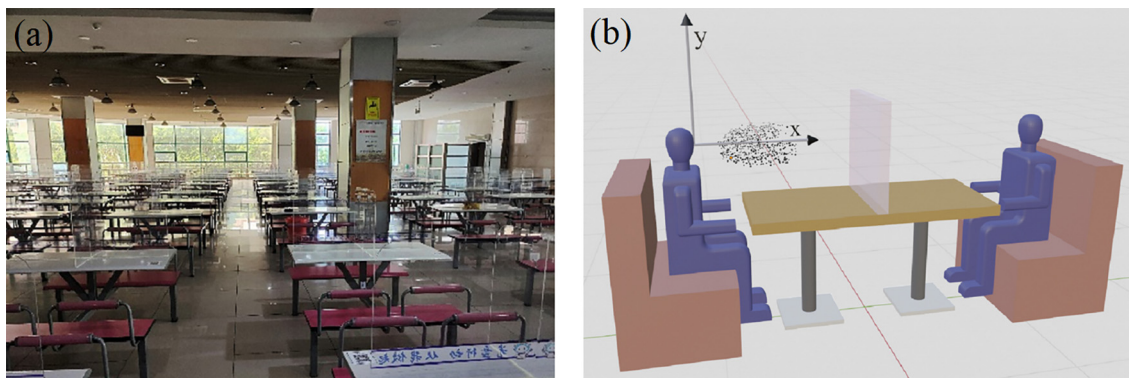


Fig. 1. Schematic of the Cartesian coordinate system for modeled dining tables and diners. (a) Dining hall with table partitions; (b) Cartesian coordinate system.

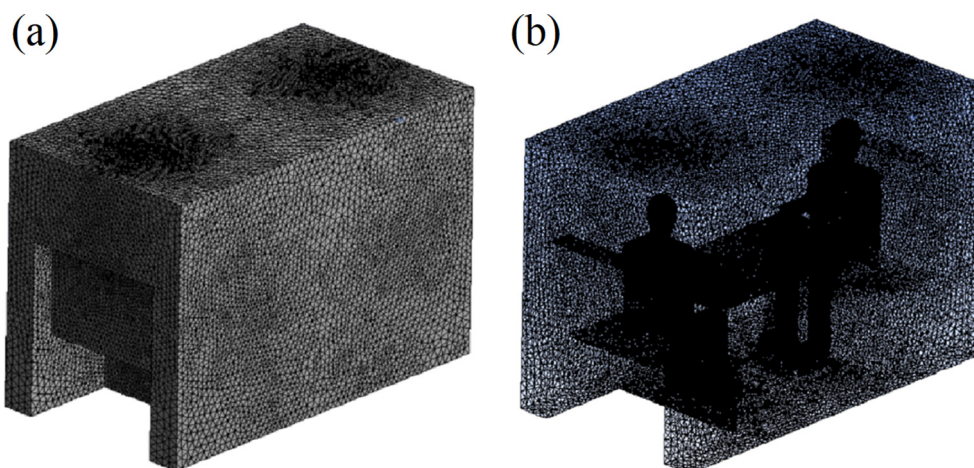


Fig. 2. Mesh views from the inside and outside of the computational domain. (a) Mesh view from the outside; (b) Mesh view from the inside.

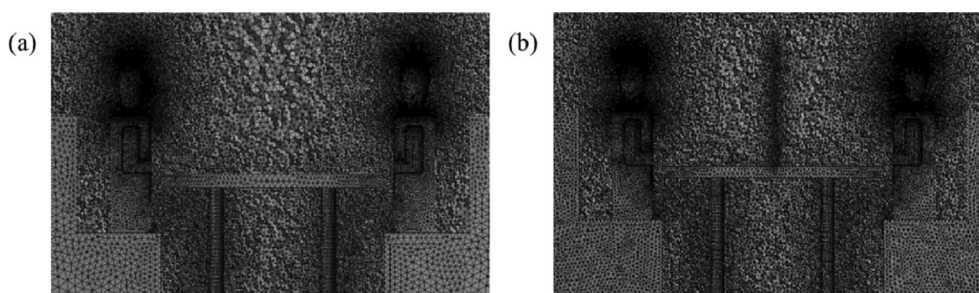


Fig. 3. Panoramic view of grid encryption. (a) Without partition; (b) With partition.

parts of the basin, larger grids were used to control the number of grids.

### 3.3. Boundary conditions and calculation parameters

The background was a restaurant with no wind inlet in the computing domain; as such, it was a static wind environment. The initial temperatures of the airflow and droplets exhaled during coughing were both set to 37 °C, which is a body temperature. To be noted here such temperature value might be higher than its real value for the airflow and droplets. The mouth was the velocity entrance, and its hydraulic diameter was 0.02 m. The cough cycle was 0.5 s, the initial speed was 11.7 m/s, and the outlet was a pressure outlet. Table 1 details the boundary condition settings.

Table 1  
Boundary condition settings in the simulation.

Boundary conditions	Parameter settings
Entry boundary type	Speed entry
Inlet velocity, m/s	11.7
Hydraulic diameter, m	0.02
Turbulence intensity	5%
Type of outlet boundary	Pressure outlet
DPM condition	Escape or trap

The formula for calculating the Reynolds number under this hydraulic diameter is as follows:

$$Re_H = \frac{\rho v d}{\mu} \tag{17}$$

In Eq. (17),  $\rho$  is the density of the fluid,  $v$  is the characteristic velocity, and  $d$  is the characteristic length. The turbulence intensity can be obtained by using the Reynolds number in the following equation:

$$I = \frac{u'}{v} = 0.16(Re_H)^{-\frac{1}{2}} \tag{18}$$

where  $u'$  is the fluctuation velocity. Chao et al. (2009) used interferometric Mie imaging technology to measure the distribution of particle size in aerosol droplets produced by a cough (Chao et al., 2009). After the analysis was simplified, particle size was fitted to a Rosin-Rammler distribution. In this study, we used their measured particle size distribution as the coughed particle size distribution from the mouth.

To verify the independence of the grid, we set the size parameters shown in Table 2. Four types of grids are generated with or without partitions, respectively. The total number of grids is 7.73, 6.67, 4.45, and 2.56 million for cases with partition, while for cases without partition the total number of grids is approximately 6.55, 5.39, 3.45, and 2.25 million.

The k-ε turbulence model is implemented under the same condition, i.e. the ambient temperature is 17 °C and the humidity is 30%, for all grids. We compare the variance of velocity along x-axis, which is shown in Fig. 4. As shown in the figure above, the curves of velocity are nearly the same for both cases with and without partitions. To make the calculation as accurate as possible, the grids of 6.55 and 7.73 million were selected for cases with and without partitions, respectively.

### 3.4. Verification of the model used in the work

To verify the accuracy of the evaporation model and the numerical calculation method, the evaporation of a single droplet in the flow field with no partitions was simulated. Table 3 presents the condition settings.

Droplets with either 10-μm or 100-μm particles were injected into the flow field. The ambient temperature was 298 K, and the

**Table 2**  
Independence verification grid generation information.

Minimum grid size (mm)	Total number of grids with partitions	Total number of grids without partitions
3	7735009	6552361
4	6672345	5397549
6	4453452	3454853
8	2569385	20254351

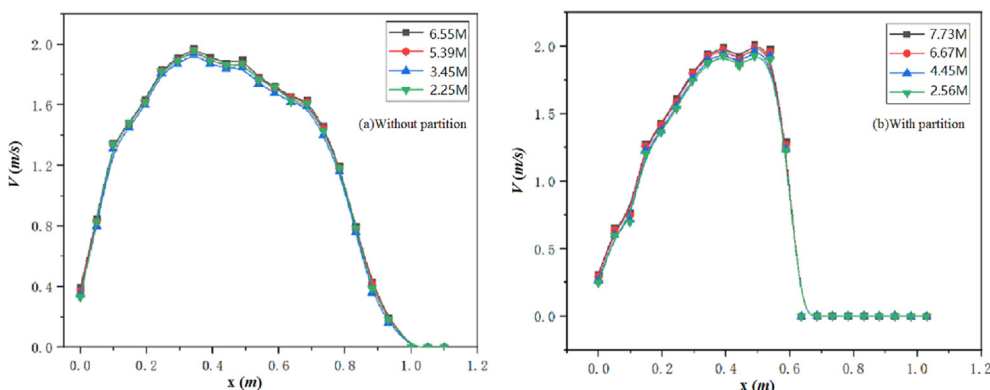


**Fig. 4.** Grid independence verification diagram.

humidity was 0%. The data on droplet size over time calculated using the dining table model were compared with data generated under the same conditions in other studies (Fig. 5). In Fig. 5, the solid orange line represents the change in diameter of the 10-μm aerosol droplets in the verification model, and the solid blue line represents the change in diameter of the 100-μm droplets. The dotted line represents the change in the size of the 10-μm and 100-μm particles during evaporation under the same conditions as in the study of Wei and Li (2015). The changes in particle size over time in the two data sets were similar, as were the curves, and the error was within a controllable range. This indicates that the evaporation model and the numerical simulation method used in this study were reliable.

**Table 3**  
Parameter settings for the verification of the evaporation model.

Calculation model and boundary conditions	Parameter settings
Turbulence model	Standard k-ε model
Speed inlet	10 m/s
Jet source type	Single
Droplet size	10 μm, 100 μm
Temperature	25 °C
Humidity	0%

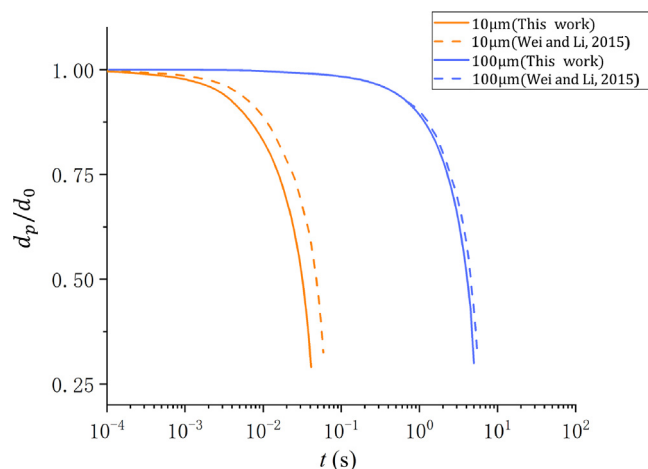


**Fig. 5.** Comparison of this work and Wei and Li (2015) for the variance of droplet size during evaporation.

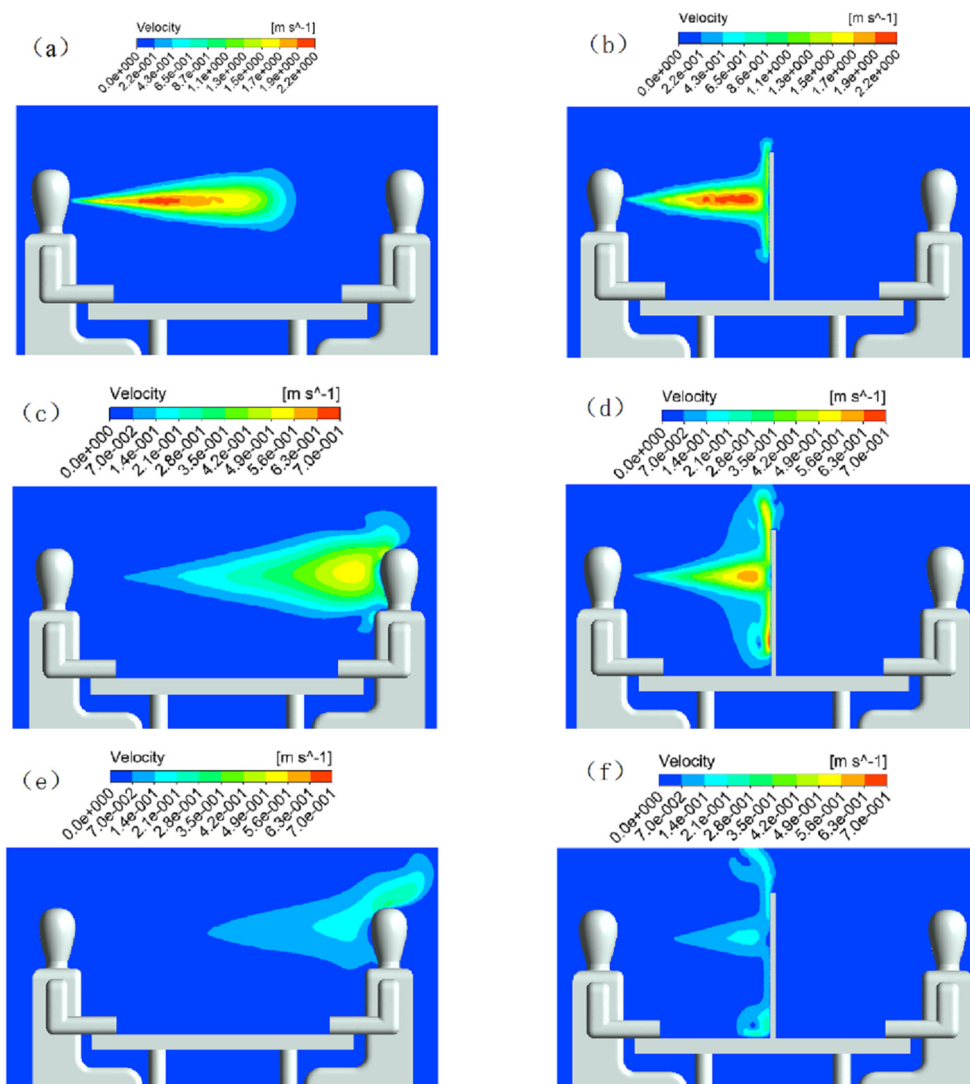


Fig. 6. x-y cross-section of velocity distribution in the flow field at 0.6, 2, and 4 s.

## 4. Results

### 4.1. Effect of partitions on the velocity field

According to the results of the numerical simulation, with a cough duration of 0.5 s, most of the aerosol droplets in the space evaporated in approximately 4 s. Therefore, we used a velocity distribution diagram that displayed the x- and y-coordinates of the flow field at 0.6, 2, and 4 s with and without partitions. Fig. 6a, c and e display the cross-sectional velocity diagrams without a partition at 0.6, 2, and 4 s, respectively. Fig. 6b, d and f display the cross-sectional velocity diagrams with a partition.

The changes in velocity in the flow field at different times indicated that without a partition, the aerosol droplets easily reached the diner on the opposite side of the table through airflow. With the partition, the velocity distribution in the flow field was concentrated in front of the partition. However, no change in velocity behind the partition was observed, and the airflow in front of the partition had a negligible influence on the velocity field behind the partition throughout the coughing process. This indicates that the partition can effectively block the air flow caused by coughing and prevent aerosol droplets from moving forward.

The nozzle entrance was used as the starting point, and the diner on the opposite side of the table was used as the endpoint. Fig. 7 presents the change in velocity between these two points over time. Fig. 7a, b and c present the change in velocity with no partition at 0.6, 2, and 4 s, respectively.

Although the maximum velocity at the starting point was 11.7 m/s, after 0.6 s, the maximum velocity in the flow field of approximately 1.8 m/s was reached in the center of the jet stream (Figs. 6 and 7). The partition strongly affected the velocity field; the direction of the velocity changed immediately after the droplets made contact with the partition (Fig. 6a and b).

Without the partition, the airflow reached the other diner at 2 s (Fig. 6c and d). At this time, the maximum velocity of the airflow was approximately 0.45 m/s. Although this velocity was low, it was sufficient to carry fine particles to the other diner. With the partition, the airflow was blocked and did not reach the other diner, and no change in the velocity in the flow field on the other side of the partition was observed (Fig. 6d). At this time, the local maximum velocity of the air mass was approximately 0.1 m/s, which is lower than the local maximum velocity of the air mass without the partition at the same time point (Fig. 7b). This indicates that the partition blocked and slowed the airflow to a certain extent.

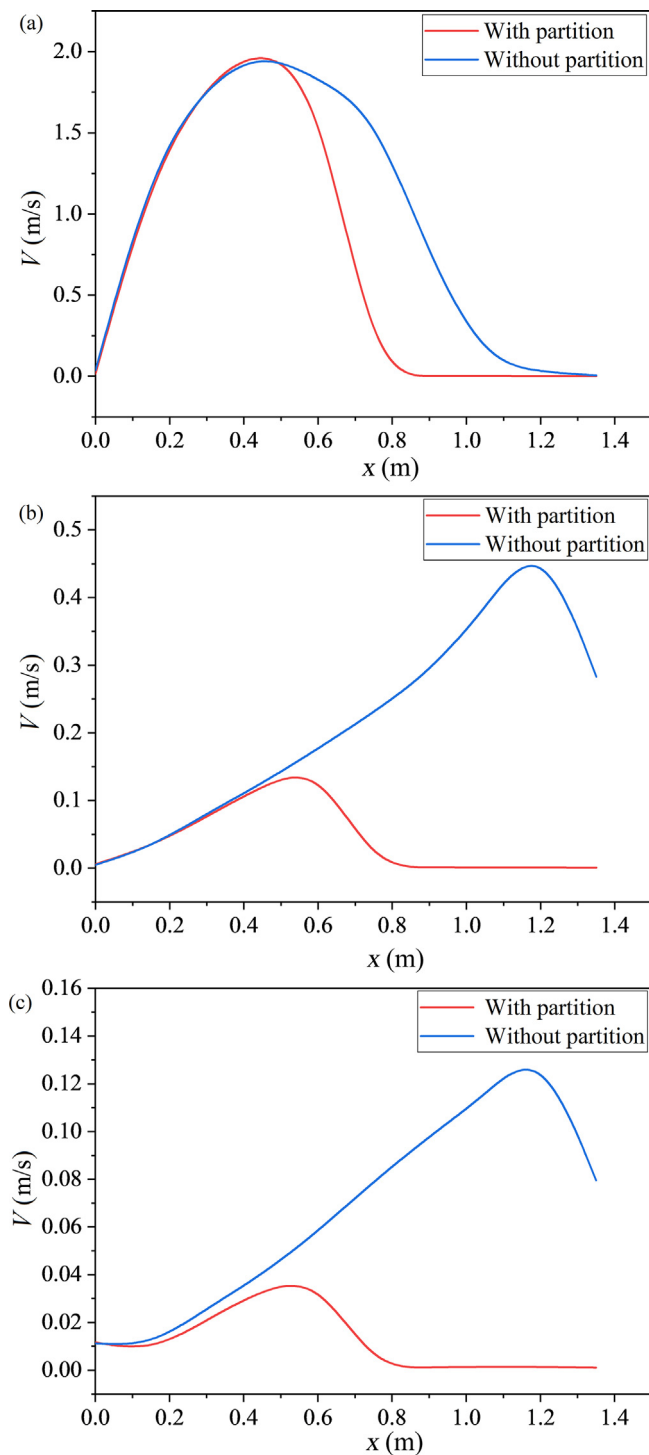


Fig. 7. Velocity variance along the line from the droplet entrance to the diner on the opposite side of the table under two different conditions.

Without the partition, the air mass generated from coughing could easily reach and even travel past the other diner (Fig. 6e and f). A partition changes the direction of airflow, and airflow speed decreases after the partition is reached.

#### 4.2. Effect of a partition on the spread of droplets

Fig. 8 presents the distribution of the aerosol droplets at 0.6 s. At this time, the aerosol droplets had not reached the other diner

but were close, and a tendency to spread to the other diner over time was observed. With partitions, only a minuscule number of droplets reached the opposite diner. Most of the aerosol droplets were blocked by the partition.

To further analyze the position of the aerosol droplets in the flow field, in this study, the  $x$ -axis in Fig. 9 was defined as the distance from one diner's mouth to the opposite diner. The particle arrival ratio,  $R_p$ , is the number of aerosol droplets that crossed coordinate  $x$  out of the total number of aerosol droplets in the flow field at a given time. Without partitions, the aerosol droplets were uniformly distributed throughout the space (Fig. 9). In the partition-free scenario (Fig. 9a), the distance between two diners was 1.35 m, and the time after a cough was 0.6 s. The longest droplet migration distance was approximately 1.28 m. With partitions (Fig. 9b), the longest droplet migration distance was 0.76 m at 0.6 s, and after this distance, the number of particles substantially decreased. Almost no droplets traveled farther than 0.8 m. This indicates that the partition blocks such droplets.

The partition effectively blocked the aerosol droplets at 0.6 s. However, at this time, the diffusion of the droplets had just begun, and the droplets had not yet diffused to the other diner. Because the effect of the partition at this time does not represent its effect over the entire course of diffusion, the distribution of the droplets must be analyzed at other time points.

Fig. 10 presents the position and particle size of the aerosol droplets in the flow field at 2 s. Without the partition, the aerosol droplets spread to the other diner, and larger particles of size 125  $\mu\text{m}$  began to settle on the dining table. With the partition, the diffusion of aerosol droplets was blocked, and only a few fine particles crossed the partition. With the partition, the particle with sizes of 125  $\mu\text{m}$  also began to settle on the table, and some of the fine (20  $\mu\text{m}$ ) particles diffused upward along with the partition.

The results of the simulations under the indicated conditions were analyzed to determine the number of particles that crossed the partition at 2 s (Fig. 11). Most of the particles traveled approximately 1.46 m, and the distance between the two diners was 1.35 m. The partition limited the movement of the aerosol droplet particles to within 0.76 m. This distance is close to that from the starting point to the partition, which indicates that the partition can effectively block the diffusion of aerosol droplets.

Fig. 12 presents the distribution of the droplets 4 s after a cough. Without the partition, most of the particles had evaporated, and the remaining droplets were approximately 50–55  $\mu\text{m}$ . Without the partition, the droplets spread from one diner to another, and a few droplets continued past the diner. This indicates that the particles can easily spread to another diner without a partition. With the partition, the aerosol droplets were blocked, and they either evaporated or settled in the flow field in front of the partition. The sizes of the droplets were similar between the two conditions, but the partition caused the distribution of the droplets to differ.

Without the partition, the maximum migration distance of the aerosol particles on the  $x$ -axis at 4 s was approximately 1.64 m, which is larger than the distance between two diners (1.35 m), shown in Fig. 13. Some aerosol droplets reached the other diner, increasing the chance of infection. With the partition, the aerosol droplet closest to the starting points was approximately 0.16 m away, and the number of particles decreased steeply after this distance. No droplets were observed beyond 0.72 m, at which point the droplet migration pattern was unclear, and evaporation was observed. Therefore, after 4 s, the migration of particles does not change substantially; evaporation and sedimentary movement are observed, but the extent is limited.

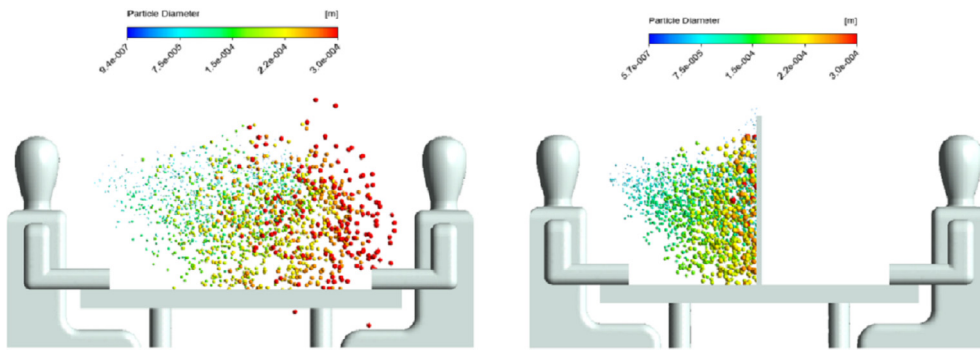


Fig. 8. Snapshot of droplets of a dinner coughing for 0.6 s.

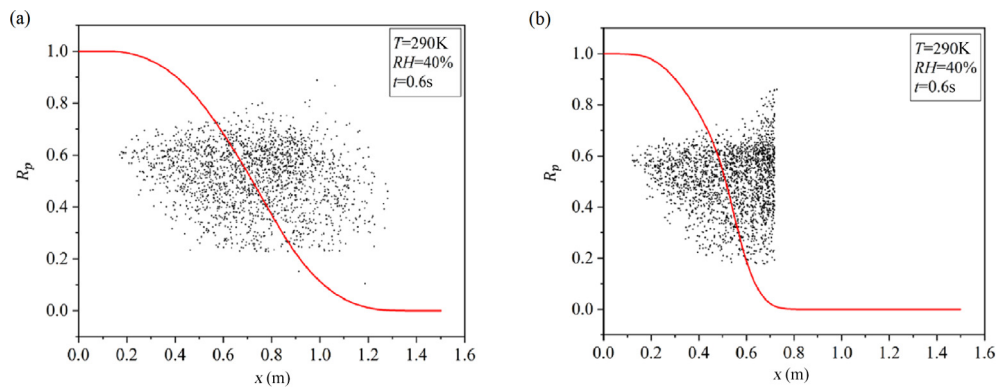


Fig. 9. The variance of  $R_p$  along  $x$ -axis after a dinner coughed for 0.6 s.

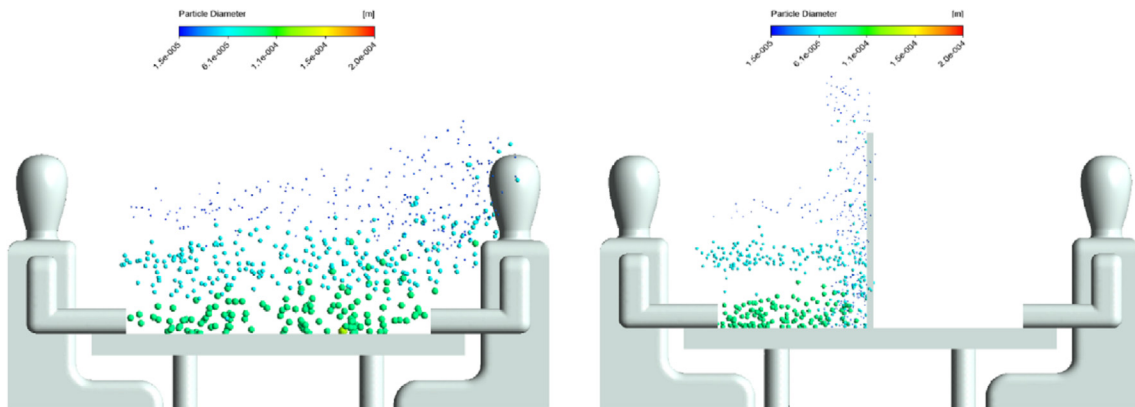


Fig. 10. Snapshot of droplets of a dinner coughing for 2 s.

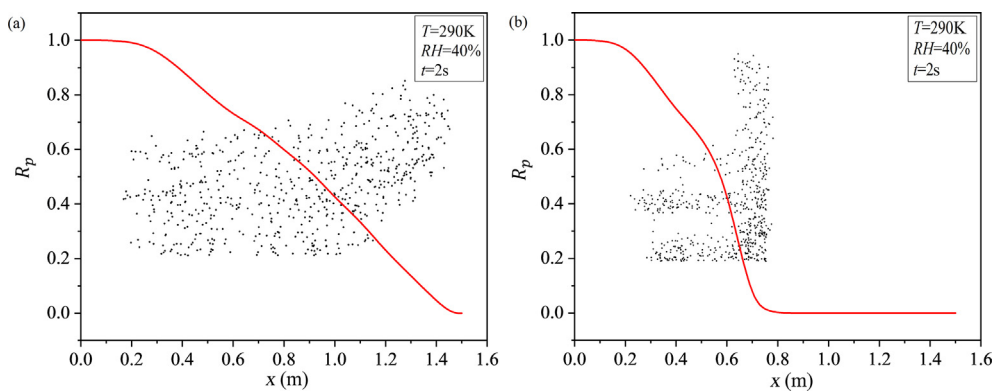


Fig. 11. The variance of  $R_p$  along  $x$ -axis after a dinner coughed for 2 s.

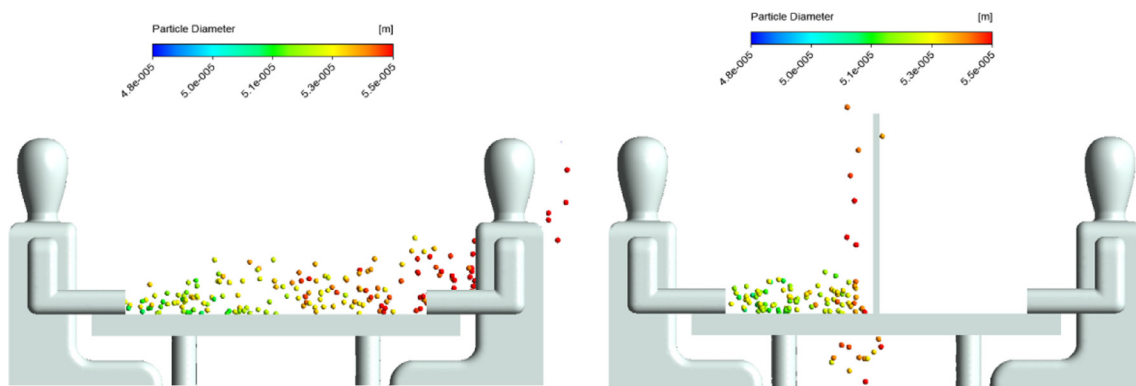


Fig. 12. Snapshot of droplets of a dinner coughing for 4 s.

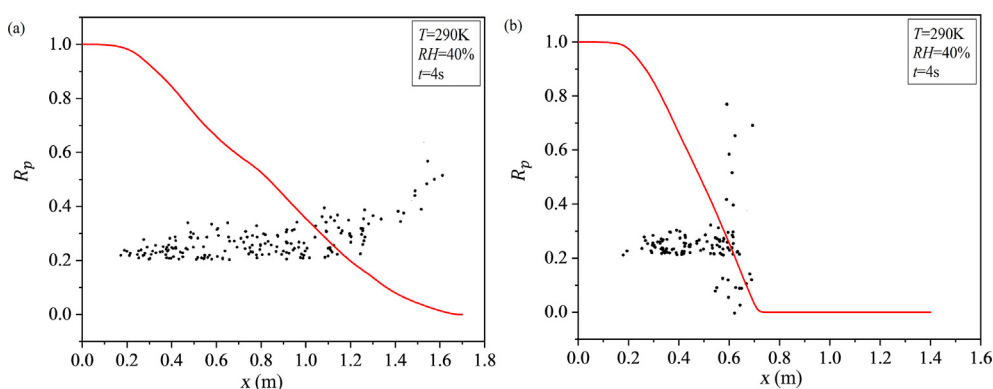


Fig. 13. The variance of  $R_p$  along  $x$ -axis after a dinner coughed for 4 s.

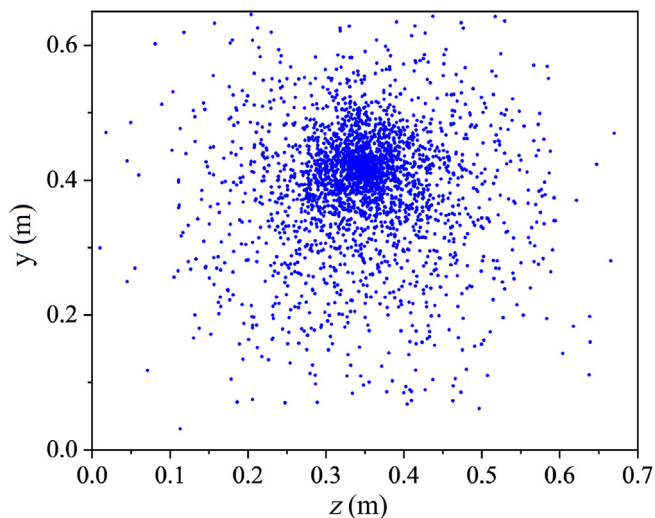


Fig. 14. Settlement snapshot distribution of aerosol droplets on the partition after a dinner coughed for 4 s.

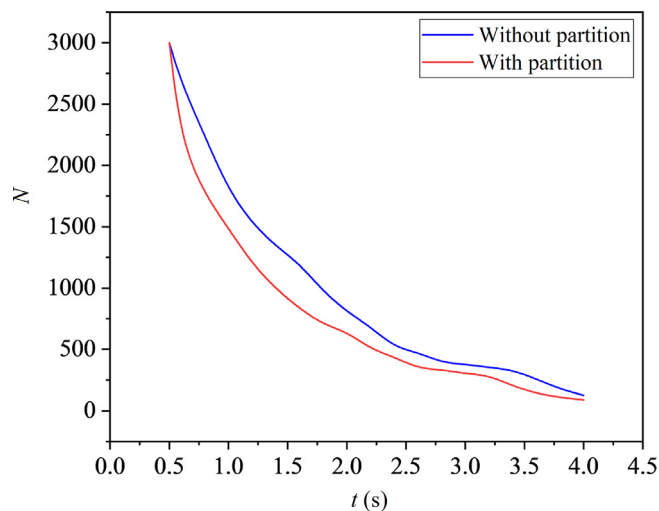


Fig. 15. The total number of aerosol droplets suspended in the air over time.

### 4.3. Collection of droplets by a partition

After the particle migration distance on the  $x$ -axis was analyzed, the effect of the partition was analyzed using the number of aerosol droplets intercepted. The aerosol particles on the partition at 4 s were analyzed, and the position of each droplet was determined using the numerical simulation. The width of the partition was

700 mm on the  $z$ -axis, and the height was 650 mm on the  $y$ -axis. The corresponding coordinate system was created. Fig. 14 presents the positions of the droplets on the partition.

The aerosol particles were densely concentrated at the center of the partition, and the droplets around the center were sparse (Fig. 15). This indicates that most of the aerosol droplets moved in the direction of cough airflow. Only a few droplets were not controlled by the airflow because of their size or turbulence and

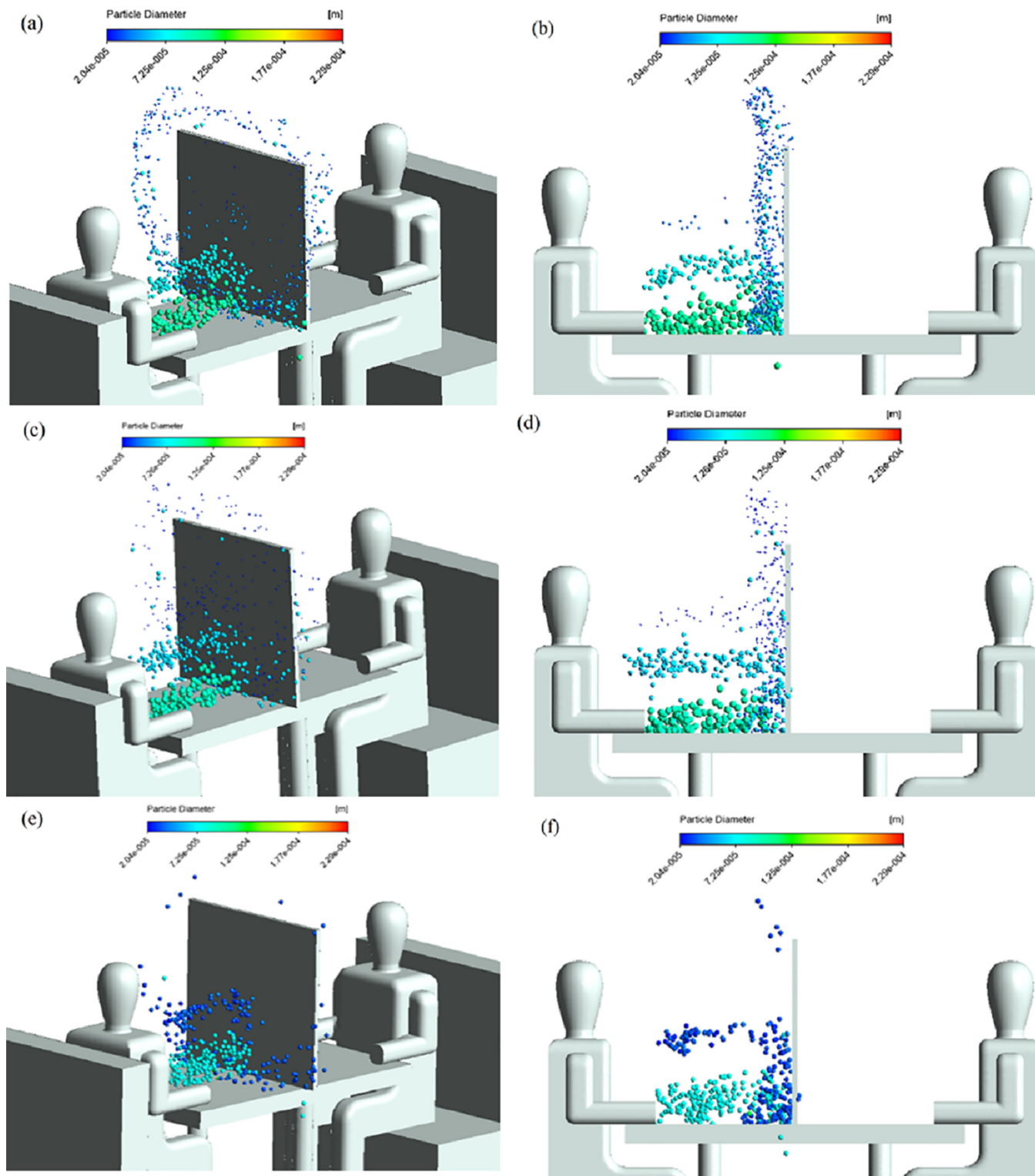


**Fig. 16.** Snapshot of droplets of a dinner coughing for 2 s. (a) 280 K space view; (b) 280 K front view; (c) 290 K space view; (d) 290 K front view; (e) 305 K space view; (f) 305 K front view.

diffused to the area beyond the partition, indicating that the partition effectively blocked most of the particles.

Fig. 15 presents the total number of aerosol droplets,  $N$ , suspended in the air over time. The droplets could have been suspended in the air, have settled on the table, or have been blocked by the partition. The number of droplets that settled on the table

was similar with and without the partition. Therefore, because the partition blocked the droplets, the number of droplets suspended in the air must have decreased. An analysis and comparison of the data indicated that because the partition blocked droplets, the number of droplets suspended in the air with the partition was lower than that without the partition until the particles

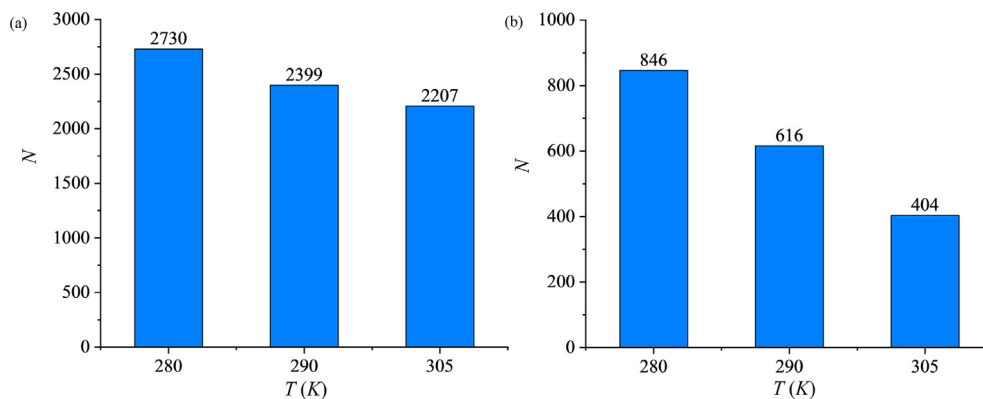


**Fig. 17.** The total number of aerosol droplets suspended in the air over time when the temperature varies at 0.6 and 2 s.

evaporated. This also indicates that the partition decreased the density of droplet distribution, thereby decreasing the distribution density of infectious viruses in the air and limiting their spread.

#### 4.4. Effect of ambient temperature on droplet diffusion

Because of the varying infectiousness of SARS-CoV-2 between seasons and climate and under different ventilation conditions of a restaurant, the ambient temperature of the restaurant was set to 7, 17, and 32 °C for winter, spring, and autumn, summer, respectively. For this simulation, a partition was used, and all other conditions remained the same; only the temperature was changed. After the literature was consulted and the local climate was considered, the temperatures were set to 280, 290, and 305 K.

Fig. 16 displays the distribution of the droplets at ambient temperatures of 280, 290, and 305 K at 2 s. As the temperature increased, the number of aerosol droplets decreased. With an ambient temperature of 290 K, the droplets near the partition were considerably smaller than those in the same position at an ambient temperature of 280 K. When the temperature was 305 K, most of the smaller particles near the partition evaporated because of the increase in the temperature, only the larger particles are left. The number of droplets suspended in the air is presented in Fig. 17, which shows the total aerosol droplets in the air decrease with an increase of temperature under the same condition. As the temperature increased, the intensity of evaporation increased, and the speed at which the aerosol droplets decrease also increased. This also indicates that an increase in temperature can inhibit the diffusion of aerosol droplets.

Many particles in the flow field had the nearly same size. To facilitate the statistical analysis and for the sake of visualization, particle sizes were divided into sections, and the number of particles in each section was counted, which is shown in Fig. 18. In this figure, the counted particle number in each section is represented by the square dot. Linear fitting was performed on the data on particle size to determine the change in the proportion of each particle size. When the temperature was 280 K, the proportion of mid-size particles was even, indicating that the particles were relatively uniformly sized and that this range accounted for a large proportion of the total particles. When the temperature was 290 K, the proportion of particle size was bimodally distributed, and the particle size corresponding to the first peak began to shift to the left, indicating that the temperature began to cause evaporation and that some of the small particles began to evaporate and decrease in size. The particles in the second peak were relatively large, and because little evaporation at this temperature was observed, the particles of this size did not change considerably. When the temperature was 305 K, the double peak disappeared, and the

curve shifted to the left relative to the 280 K curve. When the temperature was raised for the second time, the larger particles in the second peak of the 290 K plot were also affected by temperature and evaporated, and the peak began to move to the left and merge with the first peak.

This indicates that the temperature mainly affected the evaporation of the aerosol particles, which subsequently affected their diffusion distance. The simulation revealed that smaller particles were more affected by a certain temperature range, whereas the effect on large particles was small. When the temperature increased, the larger particles were affected by temperature, and the evaporation rate accelerated.

In this case, the increase in temperature inhibited the diffusion of aerosol particles. However, only pure water was used in the numerical simulation, and the effects of different temperatures on viruses were not considered. Therefore, the results only indicate that increasing the temperature can accelerate the evaporation of aerosol particles and thereby inhibit their diffusion. However, whether increasing the temperature can suppress viral aerosols remains to be determined.

## 5. Summary

In this article, a numerical method for multiphase flows is utilized to study COVID-19 aerosol transmission in a university campus food environment, which involves the generation, exhalation, and diffusion of cough droplets. The effectiveness of partitions on dining tables in a school restaurant in preventing and controlling the new coronavirus was explored by establishing a model and grid. The numerical simulation was based on the DPM, and the propagation, diffusion, evaporation, and condensation of aerosol droplets produced by coughing at a dining table in a school restaurant were simulated. The conclusions are as follows:

- (1) Partitions effectively inhibit the spread of aerosol droplets in a windless restaurant environment. The numerical simulations indicated that the aerosol droplets exhaled through coughing were blocked by the partition shortly after a cough and that the remaining aerosol particles disappeared through sedimentation and evaporation and did not reach the other diner. Therefore, partitions are effective in preventing and controlling the spread of cough droplets.
- (2) Initially, the aerosol particles were not sensitive to an increase in temperature, possibly because the particles were still controlled by the temperature of the exhaled air mass. At 2 s after the cough, the effect of temperature on the evaporation of the aerosol particles became apparent, and as the temperature increased, its effect became more pronounced.

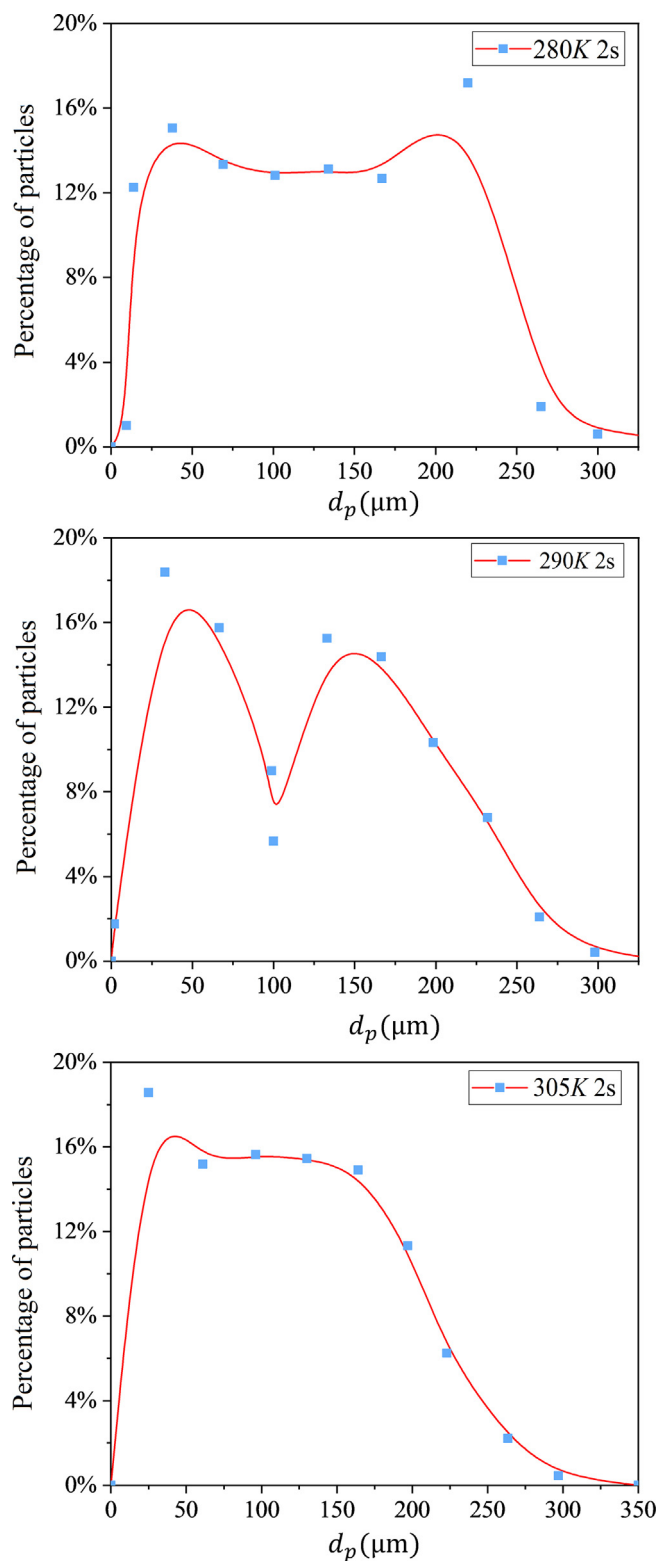


**Fig. 18.** Variance in a proportion of particle size relative to the total number of particles under different air temperatures.

When the temperature was 305 K, almost all of the particles smaller than 20  $\mu\text{m}$  in the flow field completely evaporated, and the remaining particles larger than 20  $\mu\text{m}$  were sedimented. During aerosol diffusion, the smaller droplets were the first to be affected by temperature, which caused them to rapidly decrease in size. The larger droplets were also

affected by temperature, and their size gradually decreased. The plot of droplet size distribution exhibited a single peak that transformed into a double peak and then back to a single peak.

### Declaration of Competing Interest

The authors declare that they have no known competing financial interests or personal relationships that could have appeared to influence the work reported in this paper.

### Acknowledgements

The authors thank the National Natural Science Foundation of China (11872353, 91852102) and the Natural Science Foundation of Zhejiang Province (LZ22A020004) for their support.

### References

- Bernardi, C., Chacón Rebollo, T., Hecht, F., Lewandowski, R., 2009. Automatic insertion of a turbulence model in the finite element discretization of the Navier-Stokes equations. *Math. Models Methods Appl. Sci.* 19, 1139–1183. <https://doi.org/10.1142/S0218202509003747>.
- Bourouiba, L., 2021. The fluid dynamics of disease transmission. *Annu. Rev. Fluid Mech.* 53, 473–508. <https://doi.org/10.1146/annurev-fluid-060220-113712>.
- Busco, G., Yang, S.R., Seo, J., Hassan, Y.A., 2020. Sneezing and asymptomatic virus transmission. *Phys. Fluids* 32, 073309.
- Chao, C.Y.H., Wan, M.P., Morawska, L., Johnson, G.R., Ristovski, Z.D., Hargreaves, M., Mengersen, K., Corbett, S., Li, Y., Xie, X., Katoshevski, D., 2009. Characterization of expiration air jets and droplet size distributions immediately at the mouth opening. *J. Aerosol Sci.* 40, 122–133. <https://doi.org/10.1016/j.jaerosci.2008.10.003>.
- Coronavirus disease (COVID-19): How is it transmitted? [WWW Document], n.d. URL <https://www.who.int/news-room/q-a-detail/coronavirus-disease-covid-19-how-is-it-transmitted> (accessed 8.13.21).
- Corrigan, A., Camelli, F.F., Löhner, R., Wallin, J., 2011. Running unstructured grid-based CFD solvers on modern graphics hardware. *Int. J. Numer. Meth. Fluids* 66, 221–229. <https://doi.org/10.1002/fld.2254>.
- Feng, Y., Marchal, T., Sperry, T., Yi, H., 2020. Influence of wind and relative humidity on the social distancing effectiveness to prevent COVID-19 airborne transmission: A numerical study. *J. Aerosol Sci.* 147. <https://doi.org/10.1016/j.jaerosci.2020.105585> 105585.
- Galbadage, T., Peterson, B.M., Gunasekera, R.S., 2020. Does COVID-19 spread through droplets alone? *Front. Public Health* 8, 163. <https://doi.org/10.3389/fpubh.2020.00163>.
- Galdi, G.P., 2011. *An Introduction to the Mathematical Theory of the Navier-Stokes Equations*. Springer-Verlag, New York.
- Heine, J.S., Bart, H.-J., 2017. Mass transfer during droplet formation - A measuring technique study. *Chem. Ing. Tech.* 89, 1635–1641. <https://doi.org/10.1002/cite.201700045>.
- Jamil, M., Momeni, D., Myrzakulov, R., 2012. Violation of the first law of thermodynamics in  $f(R, T)$  gravity. *Chinese Phys. Lett.* 29. <https://doi.org/10.1088/0256-307X/29/10/109801> 109801.
- Ji, Y., Qian, H., Ye, J., Zheng, X., 2018. The impact of ambient humidity on the evaporation and dispersion of exhaled breathing droplets: A numerical investigation. *J. Aerosol Sci.* 115, 164–172. <https://doi.org/10.1016/j.jaerosci.2017.10.009>.
- Li, G., Tao, W., Sun, X., 2003. Primary numerical investigation of SARS virus spreading in air. *J. Xi'an Jiaotong Univ.* 37, 764–766.
- Liu, L., Wei, J., Li, Y., Ooi, A., 2017. Evaporation and dispersion of respiratory droplets from coughing. *Indoor Air* 27, 179–190. <https://doi.org/10.1111/ina.12297>.
- Meholic, M.J., Aumiller, D.L., Cheung, F.-B., 2013. A mechanistic model for droplet deposition heat transfer in dispersed flow film boiling. *Nucl. Technol.* 181, 106–114. <https://doi.org/10.13182/NT12-10>.
- Mingotti, N., Wood, R., Noakes, C., Woods, A.W., 2020. The mixing of airborne contaminants by the repeated passage of people along a corridor. *J. Fluid Mech.* 903. <https://doi.org/10.1017/jfm.2020.671>.
- Nakano, Y., Hashimoto, A., 2020. Bubbles to Chondrites-I. Evaporation and condensation experiments, and formation of chondrules. *Prog. Earth Planet. Sci.* 7, 47. <https://doi.org/10.1186/s40645-020-00335-1>.
- Schade, W., Reimer, V., Seipenbusch, M., Willer, U., 2021a. Experimental investigation of aerosol and CO<sub>2</sub> dispersion for evaluation of COVID-19 infection risk in a concert hall. *Int. J. Environ. Res. Public Health* 18, 3037.
- Schade, W., Reimer, V., Seipenbusch, M., Willer, U., Hübner, E.G., 2021b. Viral aerosol transmission of SARS-CoV-2 from simulated human emission in a concert hall. *Int. J. Infect. Dis.* 107, 12–14.
- Sokolichin, A., Eigenberger, G., Lapin, A., Lübert, A., 1997. Dynamic numerical simulation of gas-liquid two-phase flows Euler/Euler versus Euler/Lagrange. *Chem. Eng. Sci.* 52, 611–626. [https://doi.org/10.1016/S0009-2509\(96\)00425-3](https://doi.org/10.1016/S0009-2509(96)00425-3).

Spalding, D.B., 1953. The combustion of liquid fuels. *Proc. Combust. Inst* 4, 847–864.

Wei, J., Li, Y., 2015. Enhanced spread of expiratory droplets by turbulence in a cough jet. *Build. Environ.* 93, 86–96. <https://doi.org/10.1016/j.buildenv.2015.06.018>.

Zhao, B., Zhang, Y., Li, X., Yang, X., Huang, D., 2004. Comparison of indoor aerosol particle concentration and deposition in different ventilated rooms by

numerical method. *Build. Environ.* 39, 1–8. <https://doi.org/10.1016/j.buildenv.2003.08.002>.

Zhuchkov, R.N., Utkina, A.A., 2016. Combining the SSG/LRR- $\omega$  differential reynolds stress model with the detached eddy and laminar-turbulent transition models. *Fluid Dyn.* 51, 733–744. <https://doi.org/10.1134/S001546281606003X>.